Available online at www.sciencedirect.com
ScienceDirect
Journal of the European Ceramic Society 29 (2009) 2309–2316
www.elsevier.com/locate/jeurceramsoc

The master sintering curves for $BaTi_{0.975}Sn_{0.025}O_3$/$BaTi_{0.85}Sn_{0.15}O_3$ functionally graded materials

Smilja Marković, Dragan Uskoković *

Institute of Technical Sciences of the Serbian Academy of Sciences and Arts, Knez Mihailova 35/IV, 11000 Belgrade, Serbia

Received 2 September 2008; received in revised form 21 January 2009; accepted 22 January 2009
Available online 23 February 2009

Abstract

The most important aim in the design and processing of functionally graded materials (FGMs) is to produce devices free from any deformation. Smart choices of different combination of graded layers, as well as the heating rate during sintering, are important for the fabrication of high-quality FGMs. In this study, $BaTi_{0.975}Sn_{0.025}O_3$/$BaTi_{0.85}Sn_{0.15}O_3$ (noted as BTS2.5 and BTS15, respectively) FGM was used as a model system for the construction of master sintering curves (MSCs) and estimation of the effective activation energies of sintering for different BTS graded layers. The MSCs were constructed, for BTS2.5 and BTS15 graded layers in FGMs, using shrinkage data obtained by a heating microscope during sintering at four constant heating rates, 2, 5, 10 and 20 °/min. The effective activation energies were determined using the concept of MSC; values of 359.5 and 340.5 kJ/mol were obtained for graded layers BTS2.5 and BTS15, respectively. A small difference of the effective activation energies of chosen powders made it possible for us to prepare high-quality FGMs, without delamination, distortion or other forms of defects.

Keywords: Sintering; Composites; $BaTiO_3$ and Titanates; Diffusion; Master Sintering Curve

1. Introduction

Functionally graded materials (FGMs) belong to an attractive class of materials in which it is possible to obtain a gradient of properties that cannot be attained in any monophase materials. Continuous changes in the properties of these materials for instance: composition, grain size, porosity, etc., result in the gradient of their features such as mechanical strength and thermal conductivity. Over the years, FGMs have found applications in various functional materials, like piezoelectric ceramics,[1] thermoelectric semiconductors,[2] and biomaterials.[3]

Fabrication of FGMs by powder technology is accompanied by significant problems of components' shape distortion.[4] An important processing goal for FGMs is to obtain high-quality microstructure with desired grain size and density. During the thermal treatment, different graded layers in FGM show different shrinkage kinetics, i.e. different shrinkage rates and extents of shrinkage during sintering, as well as different final density. This phenomenon can lead to excessive shape distortion, warping, delamination, development of cracks and microstructural damage in the sintered FGMs. Therefore, it is desirable to predict the sintering process (shrinkage and anisotropy) for every graded layer in FGM and design sintering strategies to achieve high-quality FGM free from any form of deformation.

Here, we have chosen BTS2.5/BTS15 FGM as a model system for the construction of MSCs and estimation of the effective activation energies of sintering for graded layers of the FGM. BTS ($BaTi_{1-x}Sn_xO_3$) powders are very important in ceramic industries. BTS powders improve the dielectric behavior of barium titanate ceramics, i.e. the increase of the Sn content (up to 15 mol%)[5] in barium titanate ceramics decreases temperature of phase transformation, and also, increases dielectric constant.[3,5–7] Furthermore, BTS powders are important for practical applications in ceramic capacitors, as well as for FGMs (in the form of monolithic ceramics with an uniaxial gradient of piezoelectric and/or dielectric coefficients). BTS FGMs are very useful because they have a broad transition temperature and high dielectric constant in a wide temperature range.[5,8] The width of the transition temperature range for BTS FGM depends on the number of layers, as well as on the tin content in each of the graded layers.[5]

* Corresponding author. Tel.: +381 11 2636 994; fax: +381 11 2185 263.
E-mail address: dragan.uskokovic@itn.sanu.ac.rs (D. Uskoković).

0955-2219/$ – see front matter © 2009 Elsevier Ltd. All rights reserved.
doi:10.1016/j.jeurceramsoc.2009.01.027

The aim of the present study has been to construct a master sintering curve for BTS2.5 and BTS15 graded layers in BTS2.5/BTS15 FGMs, for pressureless sintering using a heating microscope. FGMs were designed and fabricated by the powder-stacking method and uniaxially pressing process, followed by sintering. The shrinkage of FGMs during sintering was investigated as a function of the tin contents in the graded layers and sintering conditions. With the help of MSCs of BTS2.5 and BTS15 graded layers in BTS2.5/BTS15 FGM we can estimate the effective activation energies of BTS components. Also, we can predict the densification behavior of BTS FGM and avoid deformations of the devices.

2. Construction of the master sintering curve (MSC)

Sintering is a complex process, involving the evolution of microstructure through the action of several different transport mechanisms.[9] One of the ultimate objectives for sintering studies is to be able to predict densification results under different thermal histories for a given processing method.

Sintering kinetics of most systems of industrial importance can be quantitatively predicted by the model proposed by Su and Johnson, in which the entire sintering process is successfully described.[10] They have reported that the geometric parameters related to sintering are often functions only of density for a given powder and green-body process, provided that one diffusion mechanism dominates in the sintering process.[10] Based on that report, the concept of a master sintering curve (MSC) has been developed to characterize the sintering behavior for a given powder and green-body process regardless of the heating profiles. Using MSC, densification behavior can be predicted under arbitrary temperature–time excursions following a minimal set of preliminary experiments. These predictions can be used in planning sintering strategies. So, it is possible to make quantitative predictions of the sintering process of practical powders and, based on this, design strategies to control sintering in order to achieve high-quality products. The master sintering curve is an approach that makes it possible. Finally, the MSC is a characteristic measure of the sinterability of a compact over a wide density range.

The master sintering curve can be derived from the densification rate equation of the combined-stage sintering model.[11] For the development of master sintering curves, the parameters in sintering rate equations are separated into (a) those related to the microstructure and (b) those related to time and temperature terms, on the opposite sides of the equation, then the two sides of the equation are related to each other experimentally.[10] If there exists only one dominant diffusion mechanism (either volume or grain boundary diffusion), the terms which define the microstructural evolution are independent of the thermal history and can be represented by,[10,12]

$$\Phi(\rho) \equiv \frac{k}{\gamma \Omega D_o} \int_{\rho_o}^{\rho} \frac{(G(\rho))^n}{3\rho\Gamma(\rho)} d\rho \quad (1)$$

where k is the Boltzmann constant, γ is the surface energy, Ω the atomic volume, D_o is the preexponential factor, ρ_o is the green density of the powder compact, G is the mean grain diameter, n is the grain size power-law exponent (i.e. $n=3$ for volume diffusion and $n=4$ for grain boundary diffusion), Γ is the collection of microstructure scaling parameter.

The time and temperature dependent side of the equation can be represented as theta parameter, Θ,

$$\Theta(t, T(t)) \equiv \int_0^t \frac{1}{T} \exp\left(-\frac{E_a}{RT}\right) dT \quad (2)$$

where t is instantaneous time, which is a function of temperature, E_a is the activation energy, R is the gas constant and T is the absolute temperature. For a constant heating rate, Eq. (2) can be written as:

$$\Theta(t, T(t)) \equiv \frac{1}{c} \int_{T_o}^{T} \frac{1}{T} \exp\left(-\frac{E_a}{RT}\right) dT \quad (3)$$

where c is the heating rate and T_o is the temperature below which no sintering take place.

$$\Phi(\rho) = \Theta(t, T(t)) \quad (4)$$

The relationship between the density (ρ) and Θ (Eq. (4)) is defined as the master sintering curve. For the construction of MSC, a series of runs at different temperatures (isothermal) or constant heating rate over a range of heating rates are needed. If the activation energy of sintering is unknown, it has to be estimated in order to obtain the master sintering curve.

For the construction of MSC, the integral of Eq. (2) and the experimental density should be known. Dilatometry was conveniently used to determine the shrinkage (density) of monolayered samples.[10,12–16] However, for multilayered samples dilatometer shows total shrinkage, not shrinkage of every single layer. So, in the case of multilayered samples heating microscope, using as an optical dilatometer, can be a suitable instrument for detailed quantitative studies of sintering kinetics of each layer.[4] To the best of our knowledge, the corresponding investigations of MSCs on graded layers in FGMs were not reported until now.

For the calculation of Θ, the activation energy for the sintering process must be known. If the activation energy is unknown, it can be estimated with good precision from Θ *versus* density (ρ) data. For this purpose, a particular value of activation energy should be chosen and ρ–Θ curves should be constructed for each heating rate. If the curves fail to converge, a new value of activation energy should be chosen and the calculations repeated. This procedure should be continued until all the curves converge, showing that the activation energy is the acceptable one for sintering. A curve can be then fitted through all the data points, and then the convergence of data to the fitted line can be quantified through the sum of residual squares of the points with respect to the fitted line. The best estimate of E_a will be the value of the minimum in the plot of the activation energy *versus* mean residual squares.

Table 1
Characteristics of BTS powders.

	BTS2.5	BTS15
Formula	$BaTi_{0.975}Sn_{0.025}O_3$	$BaTi_{0.85}Sn_{0.15}O_3$
Sn content (mol%)	2.5	15
Theoretical density (g/cm^3)	6.08	6.23
Crystallite size (nm)	69.4	65.0
V (Å^3)	64.40	65.00
d_{10} (nm)	250	280
d_{50} (nm)	330	340
d_{90} (nm)	795	600
Average green density (%)	63.5	65.0

3. Experimental

The initial BTS powders ($BaTi_{1-x}Sn_xO_3$, $x = 0.025$ and 0.15, denoted as BTS2.5 and BTS15, respectively) were prepared by a conventional solid-state reaction between $BaCO_3$ (>99%), TiO_2 (rutile, >99.8%) and SnO_2 at 1100 °C during 2 h. The main characteristics of BTS powders are given in Table 1. The phase structure of the BTS powders was determined using a powder X-ray diffractometer (Philips PW 1050). Theoretical density of BTS2.5 and BTS15 powders, tin content, average crystallite size and volume of unit cell were calculated according to the Rietveld analysis on the XRD data. Rietveld analysis on the XRD patterns was carried out using the FullProf software package (version 2.10). The particle size values (d_{10}, d_{50} and d_{90}) were measured by laser particle size analyzer (PSA). The used instrument was Mastersizer 2000 (Malvern Instruments Ltd., UK), which covers the particle size range of 0.02–2000 μm. For the PSA measurements, the powders were dispersed in 2-propanol with the aid of an ultrasonic bath (low-intensity ultrasound, at a frequency of 40 kHz and power of 50 W), for 3 min. The average green density of the BTS monomorph layers, pressed in the same conditions as further FGMs, was measured according to Archimedes' principle. The average green density values of 63.5 and 65% of theoretical density were estimated for BTS2.5 and BTS15, respectively.

The BTS2.5/BTS15 FGMs were fabricated by the powder-stacking method. The BTS powders with different compositions were stacked sequentially in die; they were uniaxial pressed into cylindrical compacts (Ø 4 mm and $h \approx 2$ mm) under a pressure of 300 MPa along the thickness direction of the graded layers. The FGMs were sintered in a heating microscope (E. Leitz, Wetzlar, Germany) in order to determine the sintering shrinkage. The experiments were performed in air up to 1420 °C, using a heating rate of 2, 5, 10 and 20 °C/min. The diameters of the recorded samples were measured on appropriate images (Fig. 1(a)) of considerable enlargement, using by *measure tools* (in *pixel* units) of computer program Adobe® Photoshop® CS (version 8.0). Measurements were done on the basis of the squares grid built in heating microscope chamber (width of two squares is 1 mm). According to several measurements of every digital photograph it is established that measurement unit (1 mm) corresponds to 315–320 pixels. Measurement error was 5 pixels, i.e. less than 2%. Fig. 1(b) shows schematically the layered structure of the investigated samples. The changes of diameters (d_{bottom} and d_{top}, denoted as diameters of graded layers BTS2.5 and BTS15, respectively, see Fig. 1(b)) were photographed during sintering process at appropriate time intervals.

The microstructure of the FGMs was studied by scanning electron microscopy (SEM model JSM 5300, operating at 30 kV). Before SEM measurements, the FGM samples were cut perpendicularly with respect to the layers; the cross-section surfaces were polished and gold coated.

4. Results and discussion

The properties of the BTS2.5 and BTS15 powders are summarized in Table 1. The values of particle size and theoretical density are important because they determine activation energy for sintering process.

4.1. Sintering

It has been shown that the heating microscope is an excellent instrument for detailed quantitative studies of sintering kinetics.[4,17–19] *In situ* monitoring of the shrinkage process without the exertion of external loads is possible, so that friction with constrains and other external influences are minimized.[4]

Here, the sintering shrinkage of cylindrical compacts was recorded in radial (d) direction. From experimental data for d_{bottom} (BTS2.5), and d_{top} (BTS15) recorded at appropriate time intervals during the experiments and using Eq. (5), the percent-

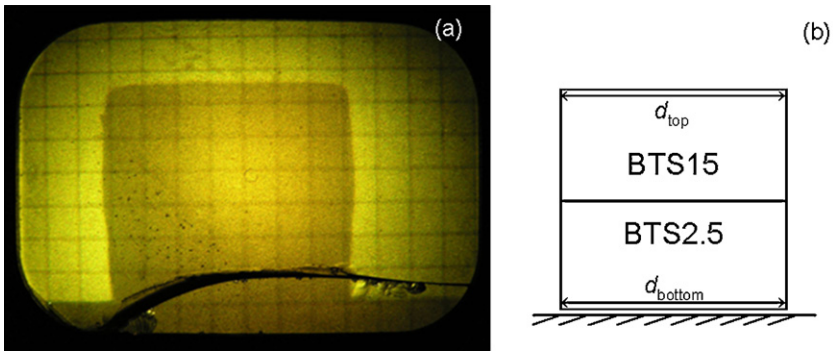

Fig. 1. (a) Photograph of sintered cylindrical sample as observed in heating microscope and (b) scheme of uniaxially pressed layered sample (after sintering denoted as BTS FGM), with marked diameters measured during sintering.

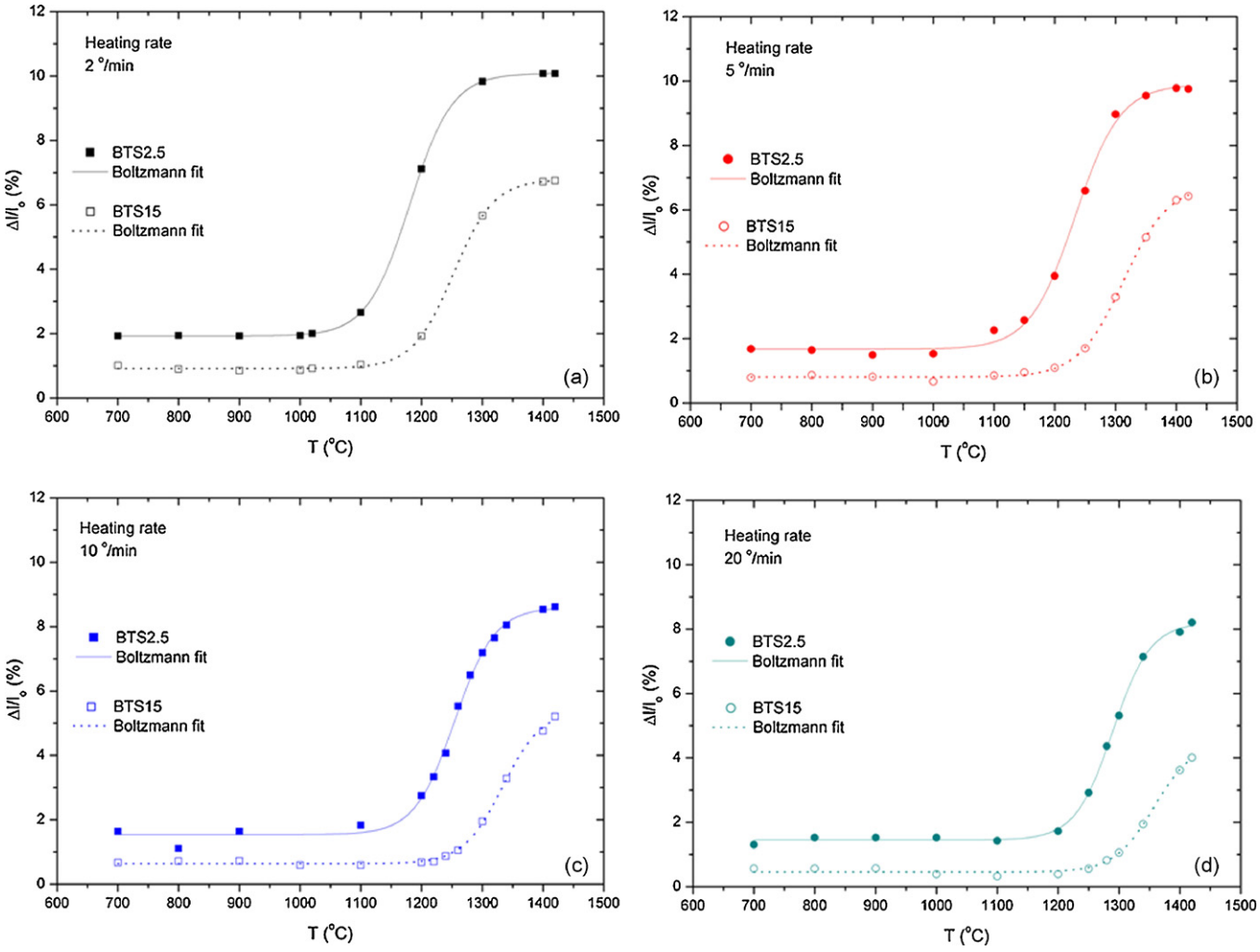

Fig. 2. Shrinkage of BTS graded layers in FGMs during different heating rate of sintering: (a) 2; (b) 5; (c) 10 and (d) 20 °/min.

age of shrinkage was calculated for the diameter of graded BTS layers in FGMs:

$$\text{Shrinkage}\,(\%) = \frac{\Delta d}{d_o} \times 100 \tag{5}$$

where Δd denotes the difference between the initial value of diameter d_o (at time t_o) and the values of d_i (at time t_i).

The calculated values of shrinkage were used for the determination of sintering behavior of FGMs graded layers. In Fig. 2, the

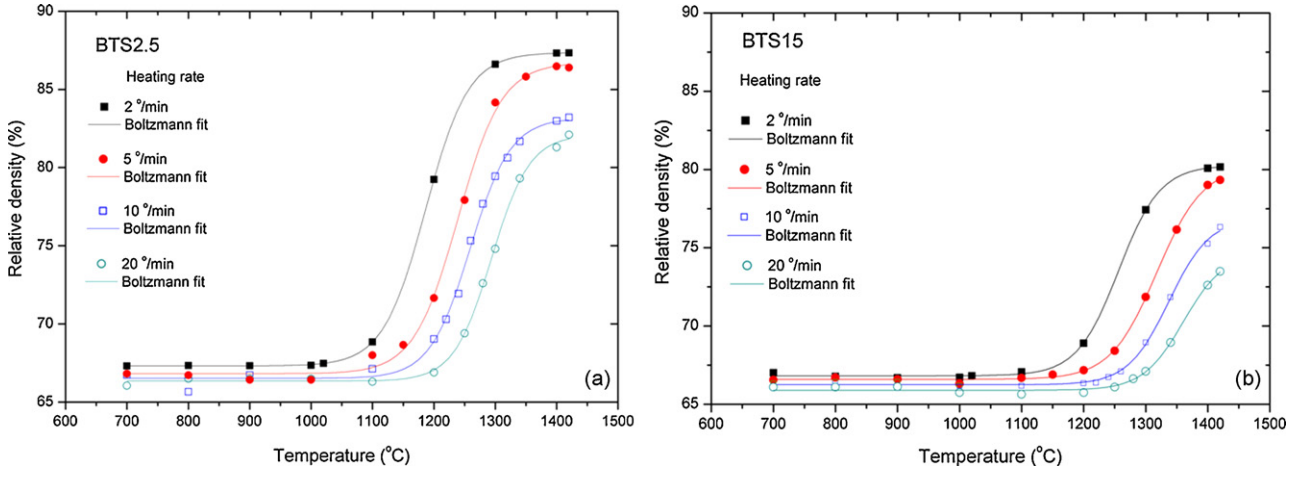

Fig. 3. Relative density (% TD) *versus* temperature for: (a) graded layer BTS2.5 and (b) graded layer BTS15, in BTS2.5/BTS15 FGM.

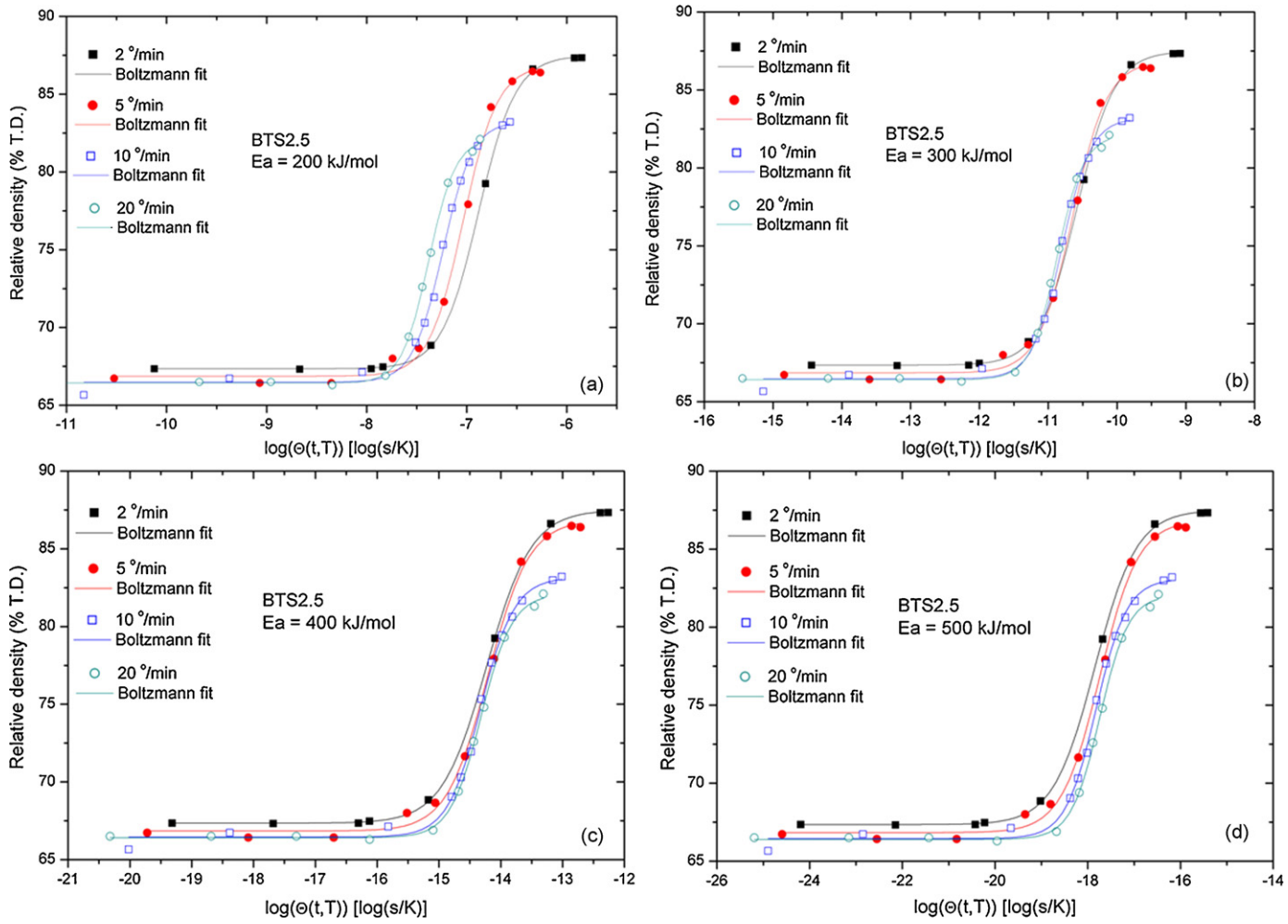

Fig. 4. $\Phi(\rho) = \log \Theta(t, T(t))$, for different E_a, for graded layer BTS2.5.

sintering behavior of FGMs was represented by the shrinkage curves of the diameter of each graded layer, BTS2.5 (d_{bottom}), and BTS15 (d_{top}) *versus* temperature during sintering. Heating rate of sintering was: (a) 2; (b) 5; (c) 10 and (d) 20 °/min.

Here, according to Fig. 2, we can compare the shrinkage behaviors of the BTS graded layers in FGMs during different thermal treatments (2, 5, 10, and 20 °/min). The shrinkage curves are relatively similar for all FGMs and both graded layers, they show that the main densification proceed in the temperature interval 1000–1300 °C (during solid-state sintering), followed by a gentle increase of the shrinkage values (slight densification proceeded with grain growth). From Fig. 2(a) it can be noticed that during the sintering with the heating rate of 2 °/min, the shrinkage of graded layer BTS2.5 begins at ∼1000 °C, and reaches the maximum value of 10%. Besides, the shrinkage of graded layer BTS15 begins at ∼1100 °C, and reaches the maximum value of 6.7%. During the sintering with the heating rate of 5 °/min, the shrinkage of graded layer BTS2.5 begins at ∼1050 °C, and reaches the maximum value of 9.8%, while, the shrinkage of graded layer BTS15 begins at ∼1150 °C, and reaches the maximum value of 6.4% (Fig. 2(b)). As it can be seen from Fig. 2(c), during the sintering with the heating rate of 10 °/min, graded layer BTS2.5 begins to shrink at ∼1100 °C, while the maximum of shrinkage reaches the value of 8.6%, in the same time, the upper part of the FGM, graded layer BTS15 begins to shrink at ∼1220 °C, while the maximum of shrinkage reaches the value of 5.2%. Finally, during the sintering with the heating rate of 20 °/min (Fig. 2(d)), the shrinkage of graded layer BTS2.5 begins at ∼1150 °C, and reaches the maximum value of 8.2%, as well, the shrinkage of graded layer BTS15 begins at ∼1250 °C, and reaches the maximum value of 4%.

Evidently, shrinkage is the most intense for the graded layers in FGM heated by 2 °/min. The degree of densification of the graded layers decreases with the increase of FGMs sintering heating rate. Also, with the increase of heating rate, the temperature at which shrinkage begins is shifted toward higher temperatures. These results confirm that the kinetics of densification of the graded layers within the same FGMs depend on heating rate.

Regardless the heating rate during sintering process, there is always a difference in shrinkage between graded layers BTS2.5 and BTS15. BTS2.5 graded layer shows the higher value of shrinkage than BTS15 graded layer in BTS2.5/BTS15 FGMs. Moreover, the shrinkage of BTS2.5 graded layer occurs at the lower temperature interval. Generally, sintering shrinkage

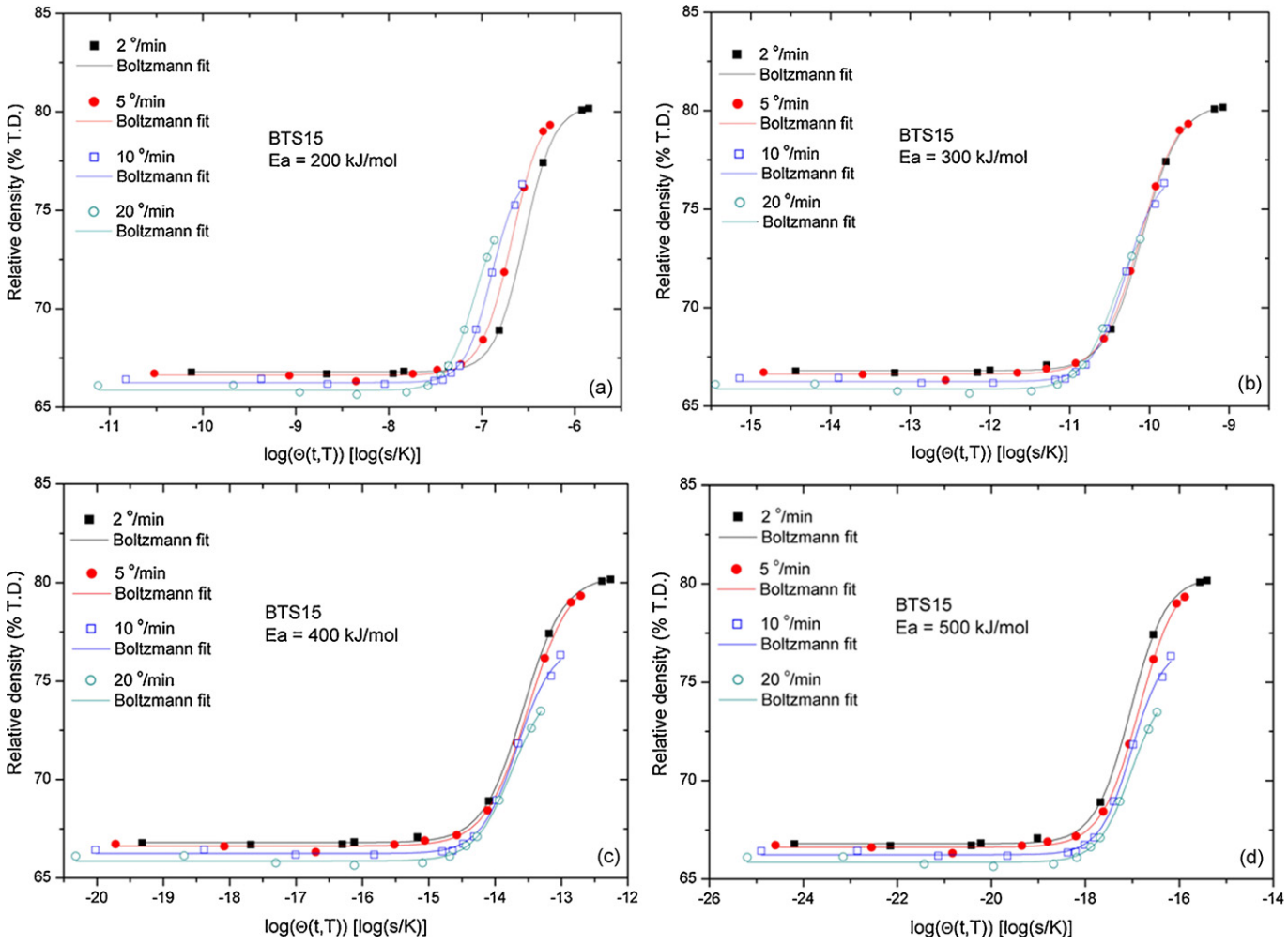

Fig. 5. $\Phi(\rho) = \log \Theta(t, T(t))$, for different E_a, for graded layer BTS15.

depends on composition, green density, temperature, time, atmosphere, etc.[20] Here, the different sintering shrinkage of the graded layers BTS2.5 and BTS15 is attributed to the difference in the tin content (i.e. composition), and can be explained by a different activation energy for sintering. Moreover, the activation energy depends on the mass transport mechanism during sintering. Thus, it is necessary to estimate activation energies for the sintering process for those two graded layers, and to find whether they are suitable for the preparation of FGMs without deformations.

4.2. Master sintering curves

Fig. 3 shows relative density *versus* temperature for (a) BTS2.5, and (b) BTS15 graded layers in FGMs sintered up to 1420 °C at the heating rates of 2, 5, 10 and 20 °C/min. The curves have similar shapes and are generally shifted to higher temperatures with increasing heating rate. It can be noted that the sintered densities obtained at any temperature showed a modest but systematic dependence on the heating rate.

By assuming isotropic shrinkage of the graded layers during sintering, the relative density was converted from the shrinkage values using Eq. (6)[13,21]:

$$\rho = \left[\frac{1}{(1 - dl/l_o)}\right]^3 \rho_o \tag{6}$$

where ρ and ρ_o are the densities of the sintered and green layer, respectively.

The use of Eq. (6) can be explained by following: if we consider whole BTS2.5/BTS15 FGMs we can notice that axial shrinkage is somewhat larger than diametrical one, thus anisotropic densification of FGMs occurs; however, there is no distinct boundary between the BTS2.5 and BTS15 graded layers in FGMs, consequently we cannot measure axial shrinkage of the layers in FGMs during sintering, i.e. we cannot consider anisotropy of the graded layers. Therefore, we assume that shrinkage of the graded layers is isotropic.

As it was noticed in part 2, one of the essential data for the construction of master sintering curve is activation energy E_a. Therefore, the density data for BTS2.5 and BTS15 graded layers obtained from the thermal microscope measurements, and values calculated from Eq. (3) are used. Firstly, ρ–Θ curves were constructed for BTS2.5 graded layer, for the four heating profiles, for a chosen value of activation energy (200 kJ/mol) as

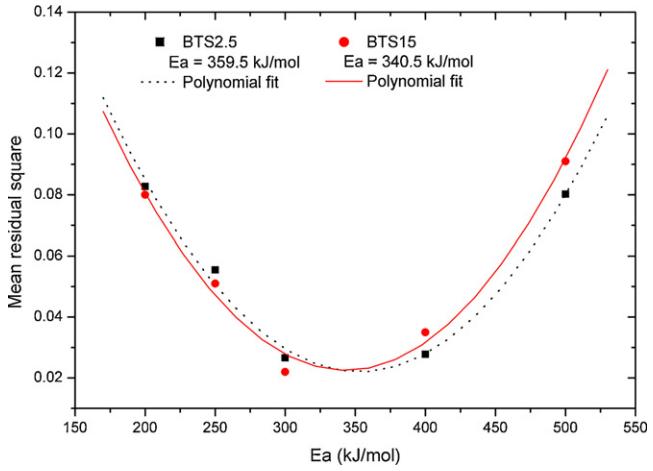

Fig. 6. Mean residual square *versus* E_a for graded layers BTS2.5 and BTS15 in BTS2.5/BTS15 FGM.

shown in Fig. 4(a). It can be seen that the curves for different heating rates are not converging. So, a new value of E_a was chosen and the calculation was repeated. The curves for 300, 400 and 500 kJ/mol are shown in Fig. 4(b–d), respectively.

The same procedure was repeated for graded layer BTS15. The ρ–Θ curves were constructed for a chosen value of activation energy (200, 300, 400 and 500 kJ/mol) as shown in Fig. 5(a–d).

Fig. 6 presents the mean residual squares for various values of the two activation energies, previously used for the construction of plots $\Phi(\rho) = \log \Theta(t, T(t))$, for graded layers BTS2.5 and BTS15. After fitting, the value of 359.5 kJ/mol was obtained as the minimum for BTS2.5 graded layer, while the value of 340.5 kJ/mol was obtained as the minimum for BTS15 graded layer.

From the knowledge of the activation energies of sintering, MSCs for graded layers BTS2.5 and BTS15 were constructed and are shown in Fig. 7. It can be seen that the value of θ, for BTS2.5 graded layer, increased from 10^{-18} at 66% of T.D. to 10^{-11} at 87.5% of T.D. Despite a 10 fold rise in heating rate, the

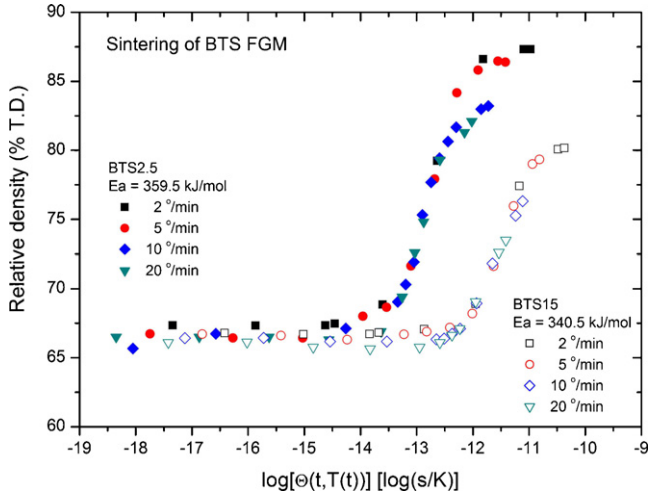

Fig. 7. MSCs ($\Phi(\rho) = \log \Theta(t, T(t))$) of BTS2.5 and BTS15 graded layers in BTS2.5/BTS15 FGM.

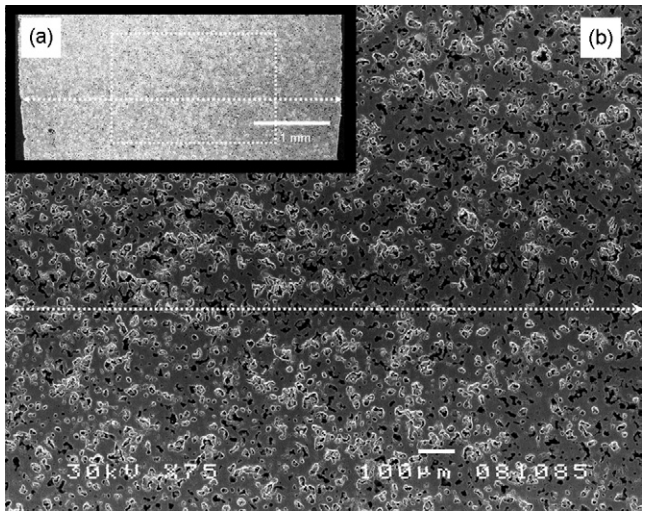

Fig. 8. Scanning electron micrographs showing: (a) macroscopic shape of the FGM and (b) magnifier BTS2.5/BTS15 boundary region. SEMs were done on polished cross-section of BTS2.5/BTS15 FGM sintered at 1420 °C, heated by rate of 10 °/min.

four sintering curves (Fig. 7, full symbols) were almost merged to one single curve, regardless of sintering path, which is defined as MSC by Su and Johnson (discrepancies between slow and fast heating rate curves, at higher densities may be caused by grain growth during which the evolution of microstructure depends on the heating profile).[10] Simultaneously, the value of θ for BTS15 graded layer, increased from 10^{-17} at 67% of T.D. to 10^{-10} at 80% of T.D. Additionally, the four sintering curves (Fig. 7, empty symbols) were merged to one single curve, regardless of sintering path.

According to these two very close and similar MSCs for graded layers BTS2.5 and BTS15 in BTS2.5/BTS15 FGM, and due to the estimated results for sintering activation energies (359.5 and 340.5 kJ/mol, respectively), delamination or distortion of FGMs are not expected during sintering up to 1420 °C. Those assumptions were confirmed by SEM analysis of BTS2.5/BTS15 FGMs in cross-section view, as shown in Fig. 8 (white dashed line marks the boundary region of the FGM). It can be seen that there is no distinct boundary between layers in BTS2.5/BTS15 FGM (Fig. 8(a)). Also, there is neither significant change of densification behavior nor microstructure in the boundary region (Fig. 8(b)). Clearly, delamination or distortion of FGMs does not exist.

According to literature data, the activation energy values for the sintering of undoped barium titanate, derived from different techniques are very scattered. The values deduced from the studies of isothermal sintering and hot-pressing fall into a range of 290–590 kJ/mol.[22–25] Those values represent the solid-state sintering mechanism. Otherwise, the activation energies from grain growth of the barium titanate ceramics were calculated to 420–840 kJ/mol.[26] Accordingly, estimated activation energies of 359.5 and 340.5 kJ/mol, for densification of BTS2.5 and BTS15 graded layers, can be ascribed to more than one mass transport mechanism operating simultaneously during the sintering process of BTS2.5/BTS15 FGMs. Therefore, since the multiple mechanisms can be active during the sintering pro-

cess of BTS2.5/BTS15 FGMs, estimated values of activation energies can be denoted as *effective activation energies*.

In the present work, during non-isothermal sintering up to 1420 °C, the FGMs have not achieved full density (about 87% of the theoretical density for the bottom—BTS2.5, and about 80% of T.D. for the top—BTS15). Using the established MSCs it is possible to find out optimal heating conditions for construction of FGMs of desired density. If the final desired density is known, it is possible to find out the corresponding θ value from the abscissa of the master sintering curve and thereafter to plan the sintering schedule. Thus, the established MSCs can be used to controlling the shrinkage behavior and also to tailoring the microstructure of BTS2.5/BTS15 FGMs. The absence of delamination and/or distortion of BTS2.5/BTS15 FGMs in any of heating conditions for construction of FGMs of desired density is provided by similarity of effective activation energies of BTS2.5 and BTS15.

5. Conclusions

It was shown that the shrinkage of BTS2.5 and BTS15 graded layers in FGMs depend on the tin content and the heating rate. BTS2.5 graded layer in FGMs always reaches higher values of shrinkage than BTS15 graded layer. Besides, identical FGMs have different sintering behavior during different thermal treatment. The percent of shrinkage of the graded layers decrease with the increase in heating rate during sintering of FGMs. Also, with increasing heating rate, temperature at which shrinkage begins is shifted toward higher temperatures. These results confirm that the kinetics of densification of graded layers within the same FGMs depend on heating rate.

The master sintering curves for BTS2.5 and BTS15 graded layers in FGMs were constructed using the shrinkage data obtained by heating microscope. The concept of MSC has been used to estimate the effective activation energy for sintering for the above composition of FGM, the values of 359.5 and 340.5 kJ/mol were obtained. Those values of the effective activation energy indicate more than one mechanism of mass transport, which simultaneously occur during the sintering process of BTS2.5/BTS15 FGMs. Neglecting differences between the effective activation energies of BTS2.5 and BTS15 graded layers enable the production of FGMs free of any form of deformation during sintering up to 1420 °C.

Acknowledgements

The Ministry of Science and Technological Development of the Republic of Serbia provided financial support under Grant No. 142006.

The authors would like to thank Prof. Dr. Đ. Janaćković for his kind help during experimental work on heating microscope.

References

1. Wu, C. C. M., Kahn, M. and Moy, W., Piezoelectric ceramics with functional gradients: a new application in material design. *J. Am. Ceram. Soc.*, 1996, **79**(3), 809–812.
2. Koizumi, M., Recent progress in FGMs research in Japan. *Int. J. SHS*, 1997, **6**(3), 295–306.
3. Chenglin, C., Jingchuan, Z., Zhongda, Y. and Shidong, W., Hydroxyapatite–Ti functionally graded biomaterial fabricated by powder metallurgy. *Mater. Sci. Eng. A*, 1999, **271**, 95–100.
4. Boccaccini, A. R., Adell, V., Cheeseman, C. R. and Conradt, R., Use of heating microscopy to assess sintering anisotropy in layered glass metal powder compacts. *Adv. Appl. Ceram.*, 2006, **105**(5), 232–240.
5. Marković, S., Mitrić, M., Cvjetićanin, N. and Uskoković, D., Preparation and properties of $BaTi_{1-x}Sn_xO_3$ multilayered ceramics. *J. Eur. Ceram. Soc.*, 2007, **27**, 505–509.
6. Yasuda, N., Ohwa, H. and Asano, S., Dielectric properties and phase transitions of $Ba(Ti_{1-x}Sn_x)O_3$ solid solutions. *Jpn. J. Appl. Phys.*, 1996, **35**, 5099–5103.
7. Yasuda, N., Ohwa, H. and Arai, K., Effect of hydrostatic pressure in barium titanate stannate solid solution $Ba(Ti_{1-x}Sn_x)O_3$. *J. Mater. Sci. Lett.*, 1997, **16**, 1315–1318.
8. Jeon, J.-H., Hahn, Y.-D. and Kim, H.-D., Microstructure and dielectric properties of barium–strontium titanate with a functionally graded structure. *J. Eur. Ceram. Soc.*, 2001, **21**, 1653–1656.
9. Uskokovic, D. P., Palmour III, H. and Spriggs, R. M., ed., *Science of Sintering. New Directions for Materials Processing and Microstructural Control*. Plenum Press, New York, 1989.
10. Su, H. and Johnson, D. L., Master sintering curve: a practical approach to sintering. *J. Am. Ceram. Soc.*, 1996, **79**(12), 3211–3217.
11. Hansen, J. D., Rusin, R. P., Teng, M.-H. and Johnson, D. L., Combined-Stage Sintering Model. *J. Am. Ceram. Soc.*, 1992, **75**, 1129–1135.
12. Su, H. and Johnson, D. L., Sintering of alumina in microwave-induced oxygen plasma. *J. Am. Ceram. Soc.*, 1996, **79**(12), 3199–3210.
13. Li, D., Chen, S. O., Sun, X. Q., Shao, W. Q., Zhang, Y. C. and Zhang, S. S., Construction and validation of master sintering curve for TiO_2 for pressureless sintering. *Adv. Appl. Ceram.*, 2008, **107**(1), 52–56.
14. Ewsuk, K. G., Ellerby, D. T. and DiAntonio, C. B., Analysis of nanocrystalline and microcrystalline ZnO sintering using master sintering curves. *J. Am. Ceram. Soc.*, 2006, **89**(6), 2003–2009.
15. Li, D., Chen, S., Shao, W., Ge, X., Zhang, Y. and Zhang, S., Densification evolution of TiO_2 ceramics during sintering based on the master sintering curve theory. *Mater. Lett.*, 2008, **62**, 849–851.
16. Garg, P., Park, S.-J. and German, R. M., Effect of die compaction pressure on densification behavior of molybdenum powders. *Int. J. Refract. Met. Hard Mater.*, 2007, **25**, 16–24.
17. Skorohod, V., Olevsky, E. and Shtern, M., Continuum theory of sintering of the porous bodies: model and application. *Sci. Sinter.*, 1991, **23**(2), 79–91.
18. Boccaccini, A. R., Sintering of glass matrix composites containing Al_2O_3 platelet inclusions. *J. Mater. Sci.*, 1994, **29**, 4273–4278.
19. Boccaccini, A. R. and Kramer, R., Experimental verification of a stereology-based equation for the shrinkage of glass powder compacts during sintering. *Glass Technol.*, 1995, **36**, 95–97.
20. German, R. M., *Sintering Theory and Practice*. John Willey & Sons, INC, New York, Chichester, Brisbane, Toronto, Singapore, 1996.
21. Kutty, T. R. G., Hegde, P. V., Khan, K. B., Basak, U., Pillai, S. N., Sengupta, A. K. *et al.*, Densification behaviour of UO_2 in six different atmospheres. *J. Nucl. Mater.*, 2002, **305**, 159–168.
22. Lin, M.-H., Chou, J.-F. and Lu, H.-Y., The rate-determining mechanism in the sintering of undoped nonstoichiometric barium titanate. *J. Eur. Ceram. Soc.*, 2000, **20**, 517–526.
23. Anderson, H. U., Initial sintering of $BaTiO_3$ compacts. *Am. Ceram. Soc.*, 1965, **48**(3), 118–121.
24. Montaghaci, H. and Brook, R. J., Kinetics of hot-pressing of $BaTiO_3$ ceramics. *Br. Ceram. Trans. J.*, 1985, **84**, 203–206.
25. Xue, L. A., Chen, Y., Cilbart, E. and Brook, R. J., The kinetics of hot-pressing for undoped and donor-doped $BaTiO_3$ ceramics. *J. Mater. Sci.*, 1990, **25**, 1423–1428.
26. Hotta, Y., Duran, C., Sato, K., Nagaoka, T. and Watari, K., Densification and grain growth in $BaTiO_3$ ceramics fabricated from nanopowders synthesized by ball-milling assisted hydrothermal reaction. *J. Eur. Ceram. Soc.*, 2008, **28**, 599–604.